Composites Part B 151 (2018) 25–34

Contents lists available at ScienceDirect

Composites Part B

journal homepage: www.elsevier.com/locate/compositesb

A crack healable syntactic foam reinforced by 3D printed healing-agent based honeycomb

Pengfei Zhang[a,b,*], Donald Joseph Arceneaux[a], Zhen Liu[c,**], Peyman Nikaeen[d], Ahmed Khattab[a,b], Guoqiang Li[e]

[a] Department of Industrial Technology, College of Engineering, UL Lafayette, Lafayette, LA 70504-2972, USA
[b] Laboratory for Composite Materials, UL Lafayette, Lafayette, LA 70504-2972, USA
[c] Terracon Consultants, Inc., Greenville, SC 29615, USA
[d] Department of Mechanical Engineering, University of Louisiana at Lafayette, Lafayette, LA 70504-2972, USA
[e] Department of Mechanical & Industrial Engineering, Louisiana State University, Baton Rouge, LA 70803, USA

ARTICLE INFO

Keywords:
Self-healing
3D printing
Syntactic foam
Smart materials
Mechanical properties

ABSTRACT

In this study, a novel grid skeleton (i.e., the 3D printed healing-agent based honeycomb structure) was embedded in a syntactic foam matrix to enable the composites to own crack closing and healing capabilities. There is always a trade-off between crack healing efficiency and overall structural properties. The new type grid skeleton was proposed here to make syntactic foam composites owning excellent crack healing ability without sacrificing overall mechanical properties. The volume fraction of glass microballoons within syntactic foam matrix remained constant at 30%. The reinforcing honeycomb cell sizes varied with a ratio from 3.8, to 5.4 and 7.3, which resulted in various physical and mechanical properties, such as different density and compressive strength. The thermal properties of the syntactic foam composites were tested through Differential Scanning Calorimetry (DSC). The interfaces between the syntactic foam matrix and PCL grid skeleton (i.e., printout) was investigated by the Fourier Transform Infrared (FTIR) spectrum. It displayed that the interaction between those phases were completely in a physical manner. Nano-indentation tests were conducted to study the composite component mechanical properties. Three-point bending tests were conducted to initiate structural level cracks to examine the crack healing capability. Healing efficiency was obtained according to the comparison between specific flexural strength before and after the crack healing event. Under free constraint condition, the 3D printed PCL honeycomb reinforced syntactic foam exhibited promising crack healing performance with healing efficiencies above 80%. This study provided an understanding on the interface property and crack healing mechanisms in the 3D printed honeycomb reinforced syntactic foam system.

1. Introduction

Syntactic foam was first developed for needs in marine and aerospace industries due to its low density [1–3]. The dispersed hollow spheres enable the foam material to have lower moisture absorption and lower thermal expansion, as a result, exhibiting excellent dimensional stability. Due to the increased application of sandwich structures in civilian and military structures, syntactic foams have been widely used as core material, and has been successfully used in multiple engineering structures for decades [4]. Such structural material was fabricated by dispersing microspheres into a polymeric or metallic matrix. The microspheres include cenospheres [5,6], phenolic microspheres [7], glass microballoons [8,9], hollow carbon microshperes [10], hollow polymer microspheres [11,12], etc. Geopolymer foams have gained new momentum partially due to the needs in eco-friendly buildings [13–15]. Energy efficiency has been recognized as the primary concern for eco-friendly buildings nowadays. In order to achieve high energy efficiency, foam concrete in which air pockets are entrapped in the mortar matrix has been widely used as fire protection and/or heat insulation material in the construction industry. The failure behavior of syntactic foam has been well studied in order to understand the cracking mechanisms [16–18]. Similar to other engineering materials, polymeric syntactic foam is also vulnerable to damage, such as impact damage, which needs repair or damage healing.

Crack self-healing is a promising concept to improve the post-impact residual bearing capacity of polymer composites [19–21].

* Corresponding author. Department of Industrial Technology, College of Engineering, UL Lafayette, Lafayette, LA 70504-2972, USA.
** Corresponding author.
E-mail addresses: pzhang@louisiana.edu (P. Zhang), zhen.liu@terracon.com (Z. Liu).

https://doi.org/10.1016/j.compositesb.2018.06.005
Received 14 February 2018; Received in revised form 28 March 2018; Accepted 4 June 2018
Available online 05 June 2018
1359-8368/

Microcapsule-based crack healing system has been well implemented in polymer composites to recover structural mechanical properties. With the help of microcapsulated epoxy and curing agents, the mechanical properties could be restored up to 80% as compared with non-damaged structural samples [22]. However, the surface approaching is always a challenge in the aforementioned system. Li and his coworkers have proposed a biomimetic two-step self-healing scheme for repeatedly healing wide-opened cracks, i.e., Close-Then-Heal (CTH) [23–27]. In such a system, the cracked surfaces approached together according to the matrix shape memory behavior. Grid stiffened syntactic foam was developed by synergizing the grid skeleton and the filled foam to improve the impact tolerance and post-impact residual in-plane compressive strength. It is worth noting that the grid stiffened structure responds to impact in a quasi-static manner. This is because each bay is small so that the flexural waves and shear waves have sufficient time to travel to and be reflected by the boundary, making peak load, deflection, and strain more or less in phase [28–30]. Syntactic foams were reinforced with SMP fibers or artificial muscles to (i) control crack propagation and (ii) narrow/close damage-induced cracks [27,31–33]. These SMP fibers and artificial muscles were configured as a grid skeleton. In order to heal the closed cracks, healing agents (soft phase) must be reinforced within polymer matrix. There is always a trade-off between crack healing efficiency and overall structural properties.

Polycaprolactone (PCL) was used as a healing agent based on physical cross-links in self-healing applications to extend lifespan of the structure [34]. It was also used to make polymer matrix owing shape memory performance [35]. 3D printing offers many advantages in the fabrication of composites, including high precision, cost effective, and customized geometry [36]. PCL honeycomb structures were successfully manufactured by the 3D printing method [37]. In this study, the 3D printed PCL honeycomb structure was embedded in a syntactic foam matrix as a new type of grid skeleton. The purpose of this study is to investigate the crack self-healing behavior of the syntactic foam reinforced by 3D printed honeycomb. The mechanical properties of the foam were studied by both in-plane and out-of-plane compression tests, along with in-plane and out-of-plane flexural bending tests.

2. Experiment

2.1. Raw materials

EPON™ Resin 862 (Hexion Inc.), which was cured by triethylenetetramine (TETA) (Huntsman Corporation LLC) for 72 h at 25 °C, was used as the foam matrix. The CAPA 6500 (Perstorp UK Ltd.), a high molecular weight thermoplastic linear polyester derived from caprolactone monomer (i.e., polycaprolactone), was used for preparing filament. It has a density of 1.1 g/cm^3 at 25 °C and melting temperature 58–60 °C. 3 M K40 glass microballoons (GMB) (3 M Inc.) with bulk density of 0.08 g/cm^3, effective density of 0.14 g/cm^3, particle diameter range of 5–200 μm, average diameter of 85 μm, and crushing strength of 1.72 MPa, were used to prepare the syntactic foam.

2.2. 3D honeycomb structure preparation

PCL filament was produced from CAPA 6500 pellets firstly. Filament tolerances created by this process, and used as printer setting test filaments were 1.75 ± 0.15 mm. The honeycomb structures were printed by the MakerBot Replicator 2X Experimental 3D Printer (MakerBot, New York City, NY). The structures were prepared with consistency in the cell wall thickness (t) while the ratio of cellular width (w) was changed to make the differentiation in cellular ratios. Through printing with equal size wall thickness, uniformity of testing results when observed on different ratio honeycombs can be controlled. Cellular width/wall thickness ratios (w/t) were found by dividing cellular width by wall thickness for each cellular array design. For instance, the smaller cellular width honeycomb structures would possess a lower ratio due to the consistent wall thicknesses, thus having higher relative density of PCL. The honeycomb cellular structure was composed of 100% infill with the PCL filament and cell width/wall thickness ratios of 3.8, 5.4, and 7.3. Important parameters for the 3D printing process discovered with testing filaments were the nozzle temperature, heated building plate temperature, print speed, and layer height. Nozzle temperature for the printer extruder was optimal at 128 °C, with a heated building plate temperature of 32 °C. Printing speed in the x-y direction was 100 mm/s, with a print layer height of 160 μm.

2.3. Syntactic foam fabrication

The 3D printed PCL honeycomb structures with dimensions of 50.8 mm × 50.8 mm × 25.4 mm were used to reinforce syntactic foam. Materials used to manufacture the syntactic foam were 3 M K40 hollow glass micro-spheres, EPON 862 Epoxy Resin, and Triethylenetetramine (TETA) curing agent. The Epoxy resin was first poured into a glass beaker, on a laboratory quality scientific scale to achieve the calculated amount of epoxy. Glass micro-spheres were then measured and poured into the beaker with the epoxy resin. The amount of glass micro-spheres added is dependent on the volume fraction desired for the application or experiment. In this study, the volume fraction of glass micro-spheres is 30% by volume. An overhead stirrer equipped with a paddle mixer was then used to mix glass micro-spheres with the epoxy for 45 min. The mixer was set to an approximate speed of 300–400 RPM (i.e., revolutions per minute). After mixing the glass micro-spheres and epoxy, TETA curing agent was added into the mixture without pausing the current mixing process. The ratio of epoxy to curing agent was 10:1. The curing agent was mixed for 3 min with the epoxy and glass micro-spheres. Upon completion of the mixing process, the beaker with the mixture was placed into a vacuum oven with no heat applied. The oven was vacuumed to −76.19 kPa (vacuum pressure) and immediately purged. This process was conducted a total of 10 times repeatedly without removing the beaker from the vacuum oven to assist in removal of air bubbles which were created during mixing. This process must be completed in a timely fashion to prevent premature curing of syntactic foam. Uncured syntactic foam was then taken out of the vacuum oven. The PCL honeycomb structures were weighed before being placed into the beaker, then the honeycomb structures were pressed into the beaker and submerged in the mixture (same orientation viewed during 3D printing). This process allows for the extremely viscous syntactic foam to occupy the interior of the honeycomb cells. The syntactic foam with the PCL honeycomb reinforcement was then poured into the aluminum mold which was lined with Teflon sheets to begin the curing process. Syntactic foam reinforced by PCL honeycomb skeleton was then allowed to cure for at least 72 h at room temperature.

The density of the foams can be calculated according to Archimedes' principles as [16].

$$\rho_c = \frac{w_a(\rho_l - \rho_a)}{0.99983(w_l - w_a)} + \rho_a \quad (1)$$

where ρ_c is the density of the composite foam (g/cm^3), ρ_l is the density of the liquid used (water, 1 g/cm^3), ρ_a is the density of air (0.0012 g/cm^3), w_a and w_l are the weight of the sample in air and liquid respectively (g). The manufactured 3D printed PCL honeycomb reinforced syntactic foams were labeled, for the sake of clarity, as SF/G3.8, SF/G5.4, and SF/G7.3. The letter “SF” represents syntactic foam composites. The numbers (i.e., 3.8, 5.4, and 7.3) are the cell width/wall thickness ratios. For example, the label of SF/G3.8 means the group sample of PCL honeycomb reinforced syntactic foam composite with honeycomb cell width/wall thickness ratio at 3.8.

2.4. Thermal properties characterization

Differential scanning calorimetry (DSC) was used to study thermal properties of the prepared 3D PCL honeycomb reinforced syntactic foam. The device used in this study is the PerkinElmer DSC 4000 (Houston, TX USA). Purging gas used was compressed nitrogen with purging rate at 20 ml/min. Temperature ranges for the DSC heating/cooling events ranged from 0 to 180 °C at a ramp rate of 10 °C/min. The sample for this experiment had a weight of 11.4 mg, with two heating events and two cooling events for testing. The second heating/cooling data sets were used for thermal property analysis.

2.5. FTIR characterization

The Fourier transform infrared (FTIR) spectrum of the composite and its components was characterized by the Agilent Cary 630 spectrometer (Agilent Technologies, CA, USA). This is to study the effect of processing on interactions between different components of the syntactic foam. Thus, samples from glass microballoons (GMB), PCL honeycomb, pure epoxy, and syntactic foam were prepared for the attenuated total reflectance-FTIR. They were tested at a resolution of 4 cm^{-1}.

2.6. Nanoindentation

The mechanical properties of different zones on the PCL reinforced syntactic foam sample were investigated by nanoindentation using a Nano indenter XP (Agila Nano indenter G200) equipped with a Berkovich diamond indenter with tip radius of about 100 nm. For preparing the sample for the nano indentation test, it was cut into small 20 mm × 10 mm × 10 mm piece and then molded in epoxy. Then, it was ground with SiC papers with grit number from 240 to 2500 and consequently polished with diamond suspension of 1.0 μm size using microcloth to achieve a mirror-shape surface finish, as shown in Fig. 1. Surface roughness is critical in performing shallow indentations and getting reliable results because it directly impacts the measured contact area between indenter and the material surface. The surface roughness of the sample were measured with Atomic Fore Microscopy (AFM) and found to be around 100 nm for the zone A and 150 nm for zone B. Ultrasonic bath was used to remove any polishing residuals from the surface of the sample which can make it difficult to measure the contact area precisely.

2.7. Compression behavior

The effect of 3D printed honeycomb reinforcement was studied by compression tests. Pure syntactic foam with 30% volume fraction GMB was prepared as a control sample. Samples were cut into 12.7 mm × 12.7 mm × 12.7 mm for the investigation on composite compression behavior according to ASTM D6641. Four specimens from each sample were prepared for compression test. Uniaxial compressive forces were applied to each test specimen using an MTS Alliance RF/100 device with a 100 kN load cell. 3D printed honeycomb reinforced syntactic foam was tested in two directions, respectively, in-plane loading direction and out-of-plane loading direction, as shown in Fig. 2. The test was executed at a loading speed of 1.27 mm/min. TestWorks 4 Software was employed to gather the data from the load cell at a frequency of 10 Hz and create a stress-strain curve for each loading cycle. Specific compressive stress σ_s was obtained by

$$\sigma_s = \sigma/\rho_c \tag{2}$$

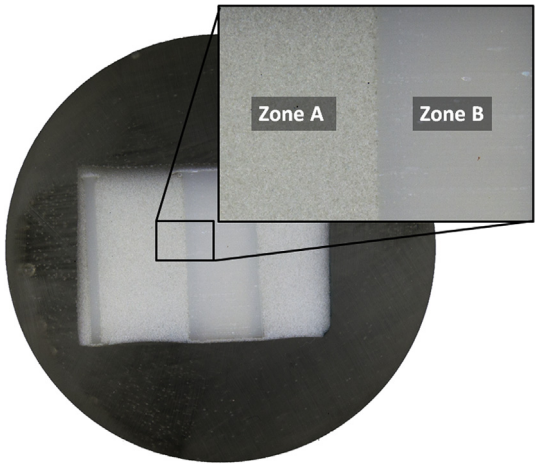

Fig. 1. Polished surface prepared for nanoindentation.

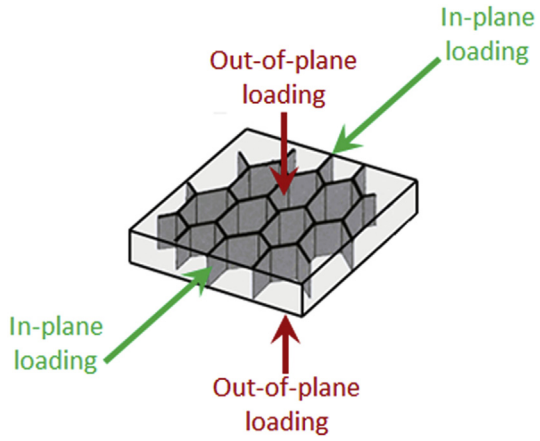

Fig. 2. Schematic of in-plane loading and out-of-plane loading diagram for syntactic foam composites under uniaxial compression.

2.8. Damage and healing inspection

In order to investigate the crack healing performance, a crack was initiated by 3-Point bending from two directions, in-plane loading and out-of-plane loading. Samples were cut to the dimensions of the honeycomb structures with a precision saw to obtain the final specimens according to ASTM D7264. The notched beam specimens were prepared in advance, with a dimension of 30 mm × 12 mm × 6 mm. The notch was machined by a circular blade saw. The depth of the notch was 2 mm. The pre-crack width was 1 mm, with a 0.5 mm crack tip radius. The purpose for using single edge notched beam specimens in this study was to create a structural scale crack. The experiment setup is shown in Fig. 3, presenting in-plane loading and out-of-plane loading under 3-point bending. The 3-point bending tests were carried out by an MTS Alliance RF/10 testing device at a loading rate of 10 mm/min. The flexural stress at the outer surface occurs at mid-span is calculated for any point on the load-deflection curve by the following equation

$$\sigma_f = 3PL/2bh^2 \tag{3}$$

$$\sigma_f^s = \sigma_f/\rho_c \tag{4}$$

where σ_f and σ_f^s are the flexural stress and specific flexural stress at the outer surface at mid-span, P is the applied force, L is the support span, b is the beam width, and h is the beam thickness. Meanwhile, the maximum strain at the outer surface occurs at mid-span could be calculated as

$$\varepsilon = 6\delta h/L^2 \tag{5}$$

where ε is the maximum strain at the outer surface, δ is the mid-span deflection, L is the support span, and h is the thickness of the beam.

The cracked samples were *in-situ* heated to 80 °C and kept at this temperature for 10 min, at a free boundary condition. They were then

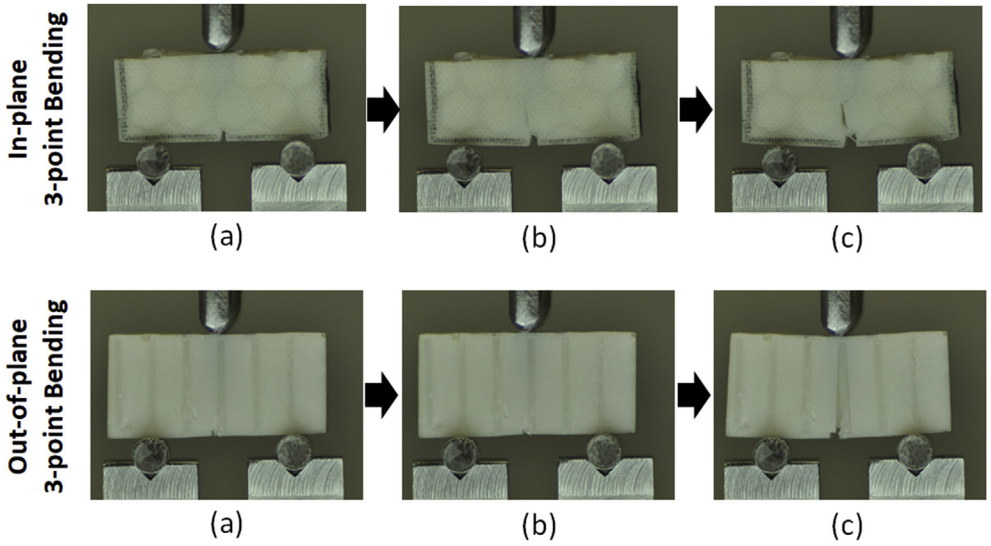

Fig. 3. In-plane and out-of-plane 3-point bending test: (a) virgin condition; (b) crack initiation; (c) crack propagation.

cooled down completely to room temperature. The repeatability of crack healing was examined by conducting 3-point bending tests on healed samples for four cycles. The crack healing efficiency η is calculated from

$$\eta = \sigma'^{H}/\sigma'^{V} \times 100\% \quad (6)$$

where σ'^{V} is the maximum flexural stress of the virgin samples, and σ'^{H} is the maximum flexural stress of the healed samples.

2.9. SEM

The fractural surfaces were studied by scanning electron microscopy (SEM). JEOL JSM-6300 field emission SEM was used in this study to obtain high-quality images. Specimens were put under a Cathode (typically Gold), and the bombardment of the gold with Argon erodes the target material onto the surface of the specimens. An accelerating voltage at 15 KV was applied to accomplish a designed magnification. Micrographs were captured with a scan speed at 35 s^{-1}.

3. Results and discussion

Tests were carried out on the prepared syntactic foams, including foam composites with and without 3D printed PCL honeycomb. Based on the tests of thermal property, FTIR, compression, bending, and crack healing, the results are discussed in the following subsections.

3.1. Thermal properties

Fig. 4 presents the heat flow curves from the second heating/cooling DSC test. There are two sharp peaks clearly exhibited on the curves. The one on the heating curve is attributed to the melting of PCL component. The peak value is 56 °C. The other on the cooling curve is attributed to the crystallization of the PCL component, with a peak at 31 °C. It also shows a step temperature change within the range of 89–95 °C, suggesting the epoxy component has a glass transition temperature at 92 °C.

3.2. FT-IR

Fig. 5 presents the infrared spectrum for syntactic foam composite and its components from 4000 to 600 cm^{-1}. An infrared spectrum of the GMB shows the amorphous Si-O-Si modes at 1250 and 1021 cm^{-1}. The transmittances at 2150, 2042, and 1980 cm^{-1} are the results of the

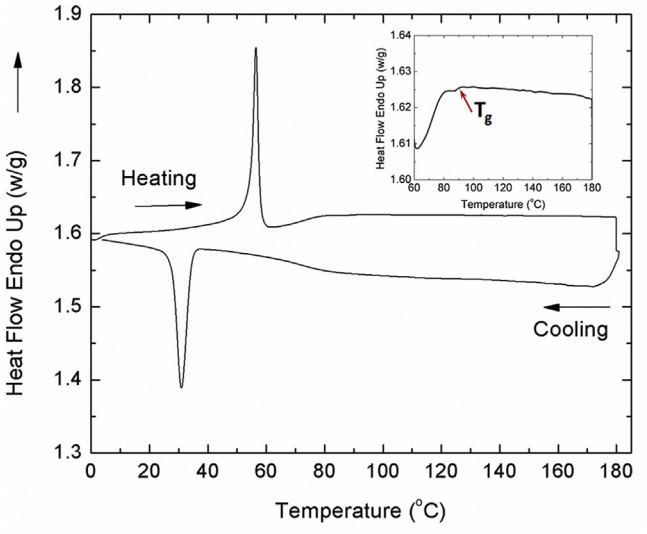

Fig. 4. Thermal property of PCL honeycomb reinforced syntactic foam (SF).

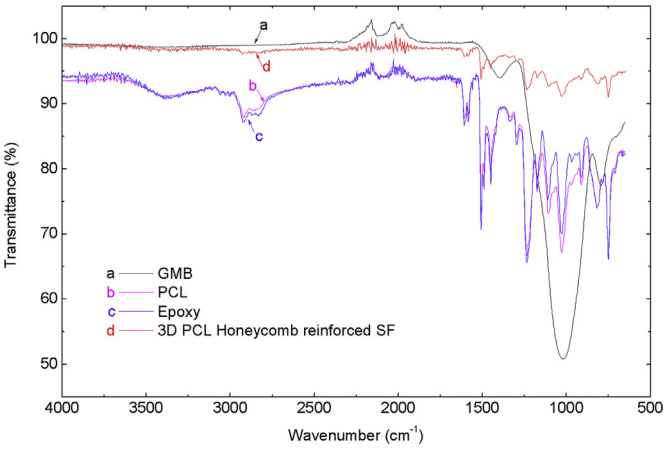

Fig. 5. FT-IR results of PCL honeycomb reinforced syntactic foam (SF) and its components.

SiH_x (x = 1, 2, 3) stretching modes [38]. At lower wavenumbers, overlap of SiH_x is observed at 799 cm^{-1}. It is worth noting that GMB is the inorganic component of the composite sample. Organic components include PCL and epoxy. Spectrums of PCL and epoxy are similar to each other from 3500 to 600 cm^{-1} except for the peaks of 1490 cm^{-1} on the epoxy curve and 882 cm^{-1} on the PCL curve, which were attributed to the N-H vibration in epoxy molecular networks and the methylene (CH_2) rocking in PCL crystalline [39,40]. As compared, the curve of 3D PCL honeycomb reinforced syntactic foam does not exhibit new peaks generated or absent peaks, indicating that the interaction between GMB \PCL\Epoxy is completely in a physical manner.

3.3. Nanoindentation

Continious Stiffness Mode (CSM) was used to measure the Young's modulus of the different locations on the sample. CSM gives modulus and hardness as a continuous function of penetration depth. Depth-control indentation was used in the CSM method with the maximum indentation depth as 10,000 nm. The tip area calibration was performed prior to the actual tests by means of 25 indentations on a reference material, fused silica (with E = 72 GPa). The harmonic displacement was set to 2 nm with a 45 Hz Frequency and the strain rate was chosen as 0.05 s^{-1}. The reason for selecting a high indentation depth was to avoid uncertainties and get reliable results as long as shallow indentations were not of interest in this study. The thickness of the sample was selected big enough to ensure that the maximum depth did not exceed a tenth of the total thickness of the sample according to the 1/10 Bückle rule of thumb [41]. The study was focused to precisely measure and compare the young's modulus of the different zones of the sample. Ten indentations were done in each zone with enough spaces between them and the data were statistically analyzed in JMP 13.0 software to study the distribution of the data and extract the mean value by performing elimination of outliers. It was observed that the average value of Young's modulus for zone A was 4.67 GPa with coefficient of variation (COV) of 3.5% and 0.67 GPa for zone b with COV of 3.7%. Fig. 6 illustrates the evolution Young's modulus (E) as a function of penetration depth for different zones of the PCL honeycomb reinforced syntactic foam sample. It can be seen that for Zone A, there are some fluctuations for the value for indentation depth smaller than 2000 nm, which was initiated from the high surface roughness and the existence of glass micro blooms in the polymer structure that makes it highly heterogeneous. For Zone B, the fluctuation is less due to the fact that the polymer is more condensed and more homogenous which results in a faster convergence of the E values. Accordingly, for calculation of the reported average E values, the data in the section of fluctuations are omitted. It is evident that the modulus of zone A is significantly bigger than the one of zone B.

Table 1
Physical properties and compression strength of syntactic foam samples.

Sample Entry		Density (g cm^{-3})	PCL Volume Fraction (%)	Specific Compression Strength (MPa.cm^3.g^{-1})
SF w/o Honeycomb		0.82	–	74.7 ± 5.9
In-plane Compression	SF/G3.8	0.92	13.2	25.1 ± 5.2
	SF/G5.4	0.91	10.6	28.9 ± 5.0
	SF/G7.3	0.89	6.9	35.6 ± 4.7
Out-of-plane Compression	SF/G3.8	0.92	13.2	57.1 ± 4.7
	SF/G5.4	0.91	10.6	62.4 ± 1.6
	SF/G7.3	0.89	6.9	58.8 ± 0.5

3.4. Compression behaviors

The volume fraction of PCL component in the syntactic foam composite can be calculated according to the component weight and composite sample weight. The physical properties such as the density of syntactic foam composite and volume fraction of PCL component are presented in Table 1. The compression tests on 3D printed PCL honeycomb reinforced syntactic foam were conducted in both in-plane loading and out-of-plane loading directions. The syntactic foam without PCL honeycomb reinforcement was used as control samples. Fig. 7 shows the compressive stresses of syntactic foam composites in the in-plane and out-of-plane directions. The specific compressive stress was determined according to Equation (2).

In a previous study, PCL particles were added and dispersed in a self-healing system as a crack healing agent [42]. It was discovered that the polymer composite samples exhibited homogeneous mechanical properties, but the strength was weakened remarkably as compared with its control sample (i.e., pure epoxy matrix). The larger the amount of the added PCL particles leads to the less the load bearing capacity. Fig. 8 shows the typical specific compression behaviors for syntactic foam samples. It clearly presents that the 3D PCL honeycomb reduces the specific compressive stress as compared with the control sample. Such decrease is remarkable if loaded in the in-plane direction. In this study, the reinforced syntactic foam exhibits heterogeneous compressive behavior. It has higher strength in out-of-plane direction than the strength in in-plane direction. It is worth noting that the architecture,

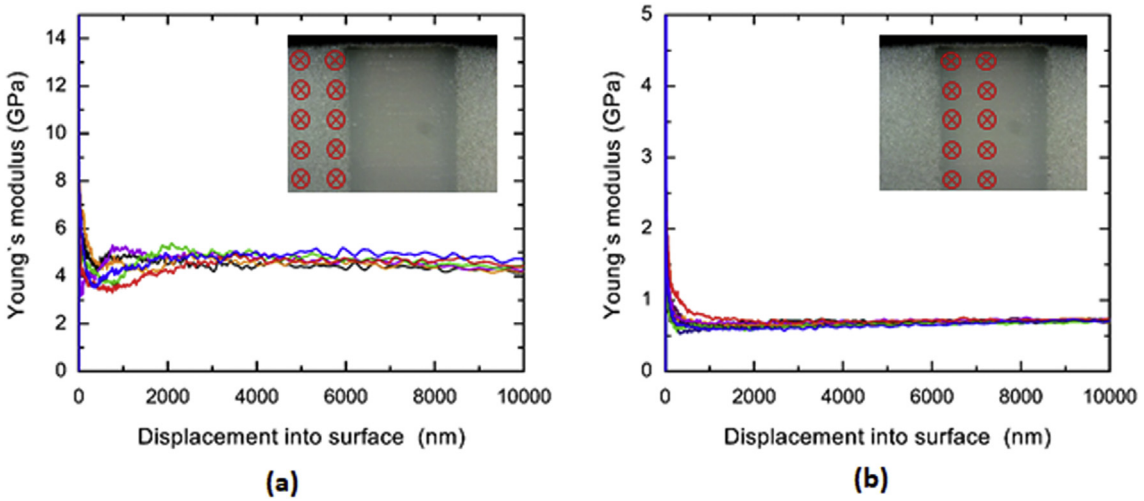

Fig. 6. Young's modulus as a function of displacement into surface for zone A and B.

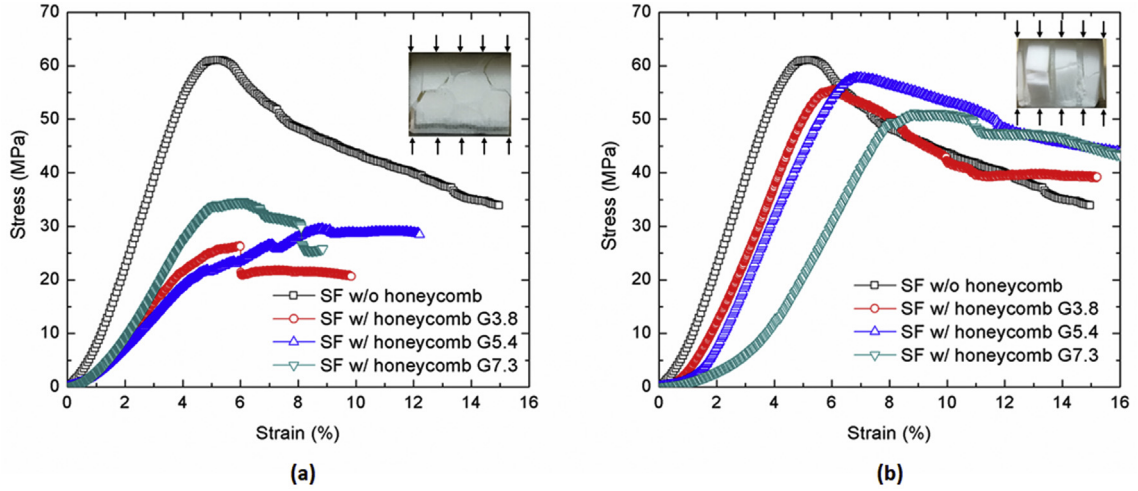

Fig. 7. In-plane compression strength (a) and out-of-plane compression strength (b) between SF w/o and SF w/honeycomb.

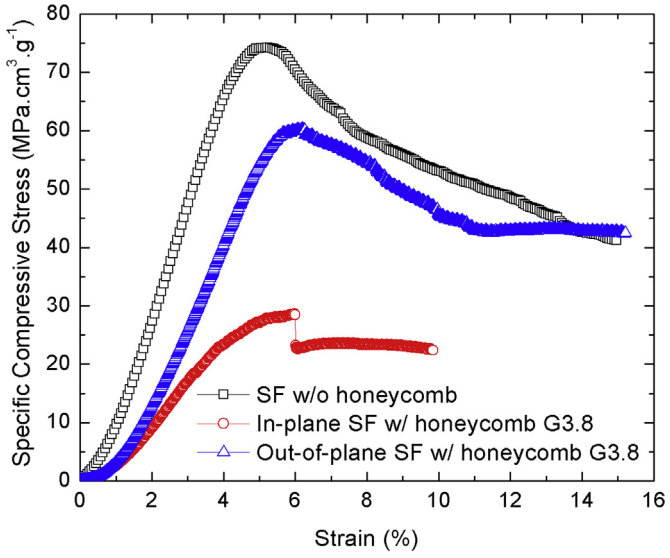

Fig. 8. Typical compression behaviors of SF without (w/o) honeycomb, in-plane SF with (w/) honeycomb (G3.8), and out-of-plane SF with (w/) honeycomb (G3.8).

based on the packing of an identical element, cannot withstand loads in the in-plane direction [43]. However, in the out-of-plane direction, the "self-lock" pattern enables the architecture possess promising load bearing capacity.

Fig. 9 shows the compression behaviors as a result of the in-plane and out-of-plane compression loading. It is interesting to see that debonding occurs at the interface between PCL skeleton and syntactic foam matrix. Fig. 10 schematically presents the representative volume element of syntactic foam composite under compression loads. As shown in Table 1, the density of the syntactic foam composite and the PCL volume fraction are related to the honeycomb cell sizes. The smaller sizes indicate the larger foam density and higher amount of reinforcing PCL. From the compression test, it suggests that the difference in cell sizes affects the in-plane compression strength; however, the variation does not affect the out-of-plane strength significantly. When under in-plane compression, as discussed earlier, the 3D printed PCL honeycomb could not bear the compression load. Acting as reinforcement, the higher amount of PCL would reduce the composite load bearing capacity, which is in agreement with what has been found from PCL particle-based polymer composites.

When under out-of-plane compression, buckling of the honeycomb cell is dominant. It is appropriate to consider the initial elastic buckling stress as the "failure" stress [44]. Due to the distributed glass microballoons, the syntactic foam matrix is compressible; while the volume of the PCL skeleton is non-compressible. It is reasonable to assume that debonding occurs when the honeycomb wall (i.e. PCL skeleton) starts to buckle, as shown in Fig. 10. In this case, the "failure" stress can be determined according to the analysis of Gibson and Ashby for honeycombs [45].

$$\sigma_z = \frac{4.5KE_s}{(1-v_s^2)\cos\alpha(1+\sin\alpha)}\left(\frac{t}{l}\right)^3 \tag{7}$$

where σ_z is the "failure" stress in the case of a syntactic foam composite under out-of-plane compression. The constant K is an end constraint factor. In this study, the depth of the honeycomb in the out-of-plane direction is much large than l. As a result, the constant K is independent of the honeycomb geometric size. The E_s is the modulus of the solid syntactic foam composite. The v_s is the Poisson's ratio of the solid syntactic foam. As pointed out by Zhang and Ashby [44], since all the cell walls have the same thickness, the geometry can be related to the relative density of the PCL honeycomb as

$$\frac{t}{l} = \frac{\rho}{\rho_s}\cos\alpha(1+\sin\alpha) \tag{8}$$

where ρ is the density of PCL honeycomb, ρ_s is the density of the solid syntactic foam composite. In this study, the angle α is 30°.

Plugging Eq. (8) into the above Eq. (7), we have.

$$\frac{\sigma_z}{E_s} = \frac{4.5K\cos^2\alpha(1+\sin\alpha)^2}{(1-v_s^2)}\left(\frac{\rho}{\rho_s}\right)^3 \tag{9}$$

The left side of Eq. (9) is the normalized strength. The compressive strength is dependent on the relative density. Fig. 11 shows the dependence of out-of-plane compressive strength on the relative density. The experimental data was calculated by normalizing the specific compressive strength in Table 1 to the specific modulus in Table 2. The obtained data exhibit good agreement with the theoretical prediction. When the relative densities are large (> 0.4), the differing in cell sizes would significantly affect the out-of-plane compression strength. In this study, the relative densities for the three groups of syntactic foam samples are low (< 0.4). Consequently, the effect of cell sizes on out-of-plane strength is not as obvious as on the in-plane strength, with regards to conclusions made from data in Table 1 or Fig. 9(b).

3.5. Flexural behaviors

Under 3-point bending test, the data of bending loads and mid-span

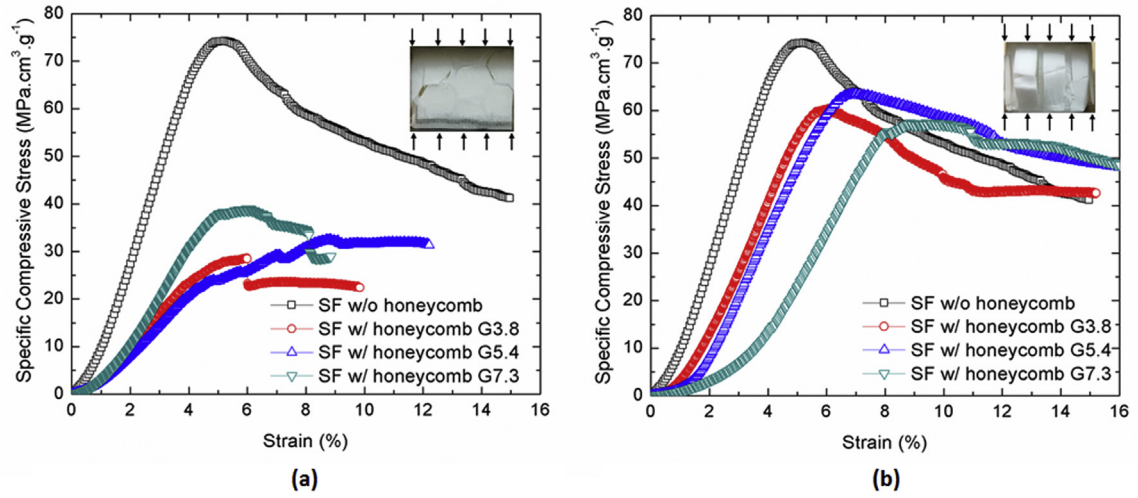

Fig. 9. In-plane specific compression strength (a) and out-of-plane specific compression strength (b) between SF w/o and SF w/honeycomb.

deflection were recorded. The specific flexural strength at the outer surface occurs at mid-span was calculated according to Eqs. (3) and (4). The flexural strength of the syntactic foam composite sample was investigated, including the in-plane and out-of-plane flexural strength. Fig. 12 shows the flexural stresses of the syntactic foam composite. The specific flexural stresses were presented in Fig. 13. The syntactic foam without 3D printed PCL honeycomb was used as control sample. The flexural behavior suggests that: (1) The control sample is brittle while the honeycomb reinforced syntactic foam is ductile. From the curves, one peak can be observed for the control sample; but for syntactic foam samples with honeycomb reinforcement, the curve does not drop after the peak. During the testing process, the control sample broke in half once the bending load reached the peak value. The other groups of samples (i.e., with honeycomb) exhibited debonding between PCL skeleton and foam matrix after the peak. The continuous loading resulted in the stretching of PCL skeleton. (2) As compared with the control sample, both flexural stress and specific flexural stress significantly decrease for those reinforced with PCL honeycomb. In addition, those stresses in the in-plane and out-of-plane situations are almost the same, which is completely different from the compression behavior. It is worth noting that a pre-crack was prepared in advance before the 3-point bending. Similar to the results under compression, the failure of syntactic foam composite is caused by the debonding. It is believed that the flexural stress or specific flexural stress for syntactic foam with honeycomb is the debonding stress. (3) As a result, regardless of the amount of PCL honeycomb reinforcement used, it would not change the specific flexural stress as long as it has the honeycomb reinforcement. This explains why the specific flexural stresses are the same for honeycomb reinforced syntactic foam composites with varied PCL volume fractions (i.e., cell sizes). It is envisioned that in order to improve the flexural strength, the focus should be directed towards enhancing the interfacial bonding between the foam matrix and PCL skeleton.

3.6. Crack healing performance

In this study, the crack was initiated by bending force. After the removal of the bending load, the cracks were narrowed because of the elastic behavior of the stretched PCL honeycomb. The “springback” behavior of the 3D printed PCL honeycomb was investigated in our

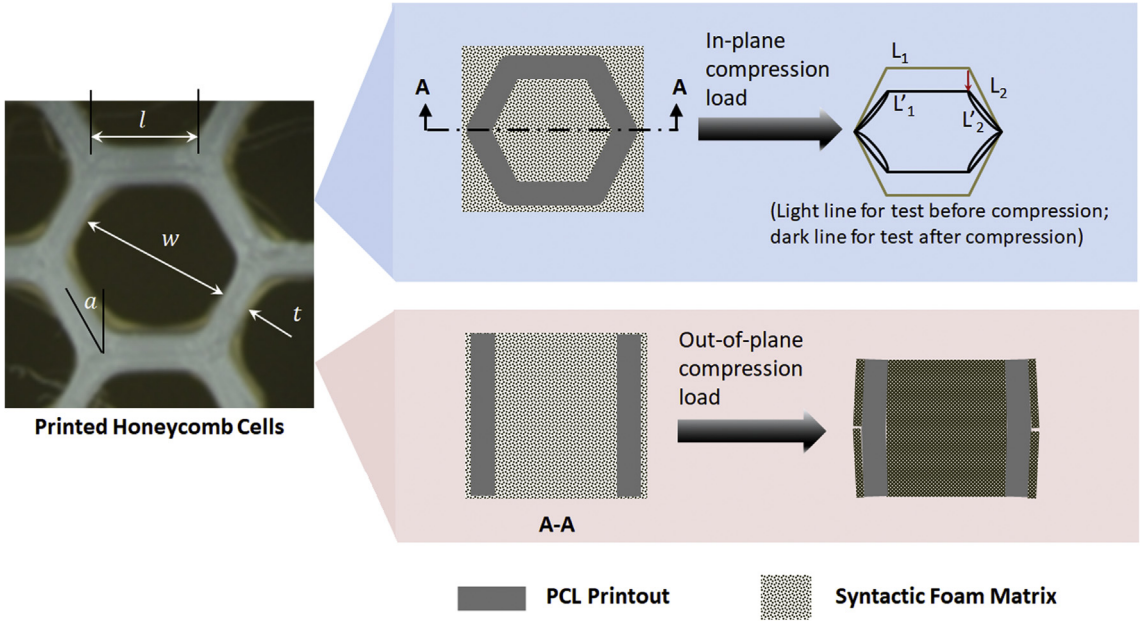

Fig. 10. Representative volume element of SF w/honeycomb (A-A is the sectional view) under in-plane and out-of-plane compression loads.

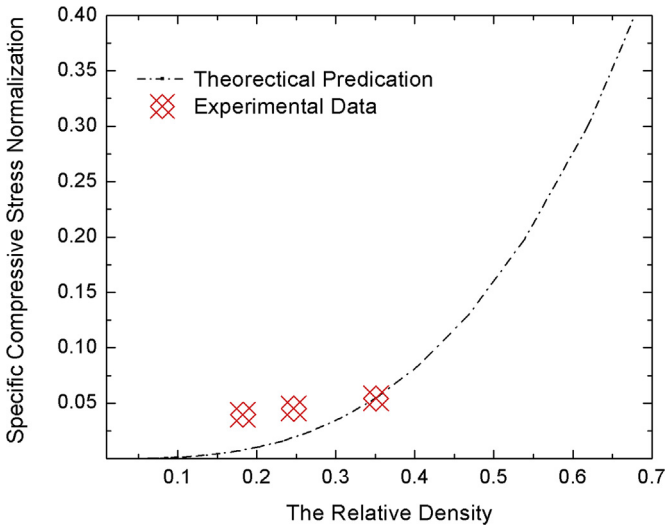

Fig. 11. The graph shows the specific compressive strength normalization in the out-of-plane direction when $K = 0.06$ and $v_s = 0.4$ [Eq. (9)]. The theoretical prediction is indicated by the dashed line.

Table 2
Geometry factors of printed PCL honeycomb and the related mechanical properties.

Sample Entry	w/t	t/l	The relative density ρ/ρ_s	Specific Modulus of the solid syntactic foam (MPa.cm^3.g^{-1})
SF/G3.8	3.8	0.24	0.18	1439
SF/G5.4	5.4	0.32	0.25	1384
SF/G7.3	7.3	0.46	0.35	1082

previous study [37]. It was deformed under compression loads, up to 70% strain. The deformed honeycomb could elastically recover back with a recovery ratio up to 81% at room temperature under free constraint condition. According to Eq. (5), all the maximum strains at the samples' outer surface occur at mid-span were within 10%. The deformation was completely within the elastic region. The bending induced crack was narrowed efficiently due to the "springback" behavior. As shown in Fig. 14, the virgin sample with a pre-crack was damaged under a bending load. The crack propagated along the interface between PCL printout and syntactic foam matrix. The crack was completely closed and healed after the thermal treatment described in Section 2.8.

The crack healing temperature was determined through DSC result analysis. The virgin and healed samples were tested under 3-point bending. The peak specific flexural stress was used to examine the crack healing efficiency. According to Eq. (6), the crack healing efficiency and repeatability were presented in Fig. 15. The data was averaged out from four tested samples. It is worth noting that the crack healing performance was investigated under static loading at room temperature. It shows that for some groups of samples, the efficiency even reached above 100% (up to 132% in some cases) in the first or second healing event. It eventually maintained above 80% after four damage-healing events. It is interesting that the healing efficiency did not show bias toward the bending load directions.

The crack healing of syntactic foam composites follows the procedures (i) surface rearrangement, (ii) surface approach, (iii) wetting, (iv) diffusion, and (v) randomization [37]. Keep in mind that the cracked composite samples were healed under free constraint conditions in this study. Among the procedures, wetting is very important for syntactic foam system. The wetted areas in a domain propagated over the entire fracture surfaces would eventually determine the crack healing efficiency. In addition, the wetting rate is also very significant for a crack healing process. As shown in Fig. 14, there are numerous cavities on the fracture surfaces because of the embedded glass microballoons. In the syntactic foam system, the melted PCL flowed randomly to open spaces and filled the broken glass microballoons, resulting in the increase in wetting area [33]. As a result, the cavity area became solid between the foam matrix and PCL skeleton, leading to a high efficiency, sometimes above 100%. The increase in wetting area would improve the healing efficiency in a second healing event. As the diffusion and molecular randomization is approached, the entire fractured surfaces would be completely wetted by molten PCL. At this stage, the thickness of the molten PCL determines the strength of the bonding interface [42]. The thicker wetting PCL leads to weaker bonding strength, thus reducing crack healing efficiency. Since the crack was narrowed by the elastic springback of PCL skeleton and healed under free constraint condition, the crack could not be closed completely but filled with wetting PCL. Such a wetting PCL layer became thicker one event after another. This explains the healing efficiency increase in the second event but decreased in the following healing events. In some cases, the healing efficiency dropped after the first healing event and kept dropping. This is due to the different wetting rates. Higher wetting rates indicate that the entire fractured surfaces would come into contact with molten PCL in a shorter timeframe. The wetting rate depends on different stages of PCL crack-filling, which are instant wetting, constant rate wetting, and Gaussian wetting. The modes of wetting rates in this study are not investigated, which could be a potential research topic in the future.

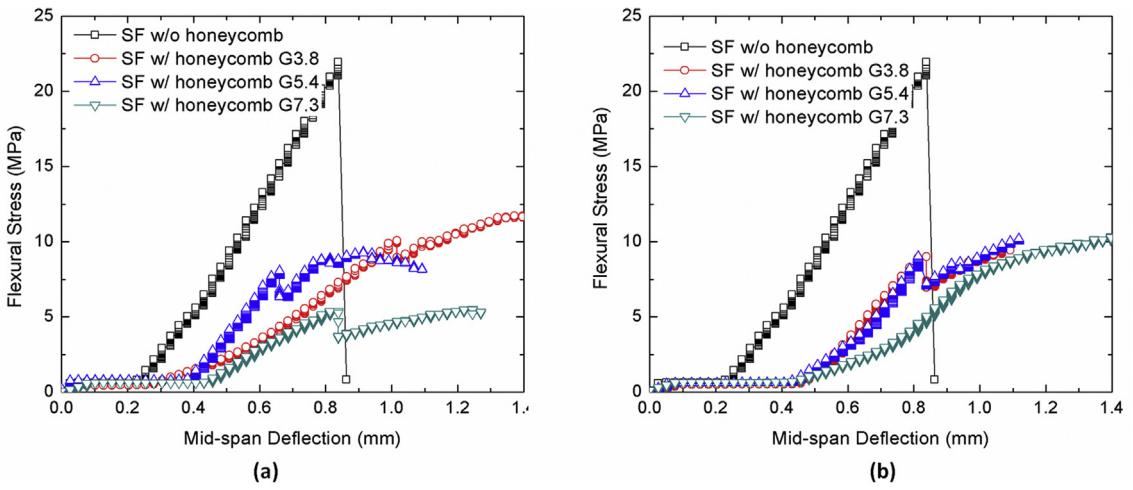

Fig. 12. Flexural strength of syntactic foam composites under in-plane 3-point bending (a) and out-of-plane 3-point bending (b).

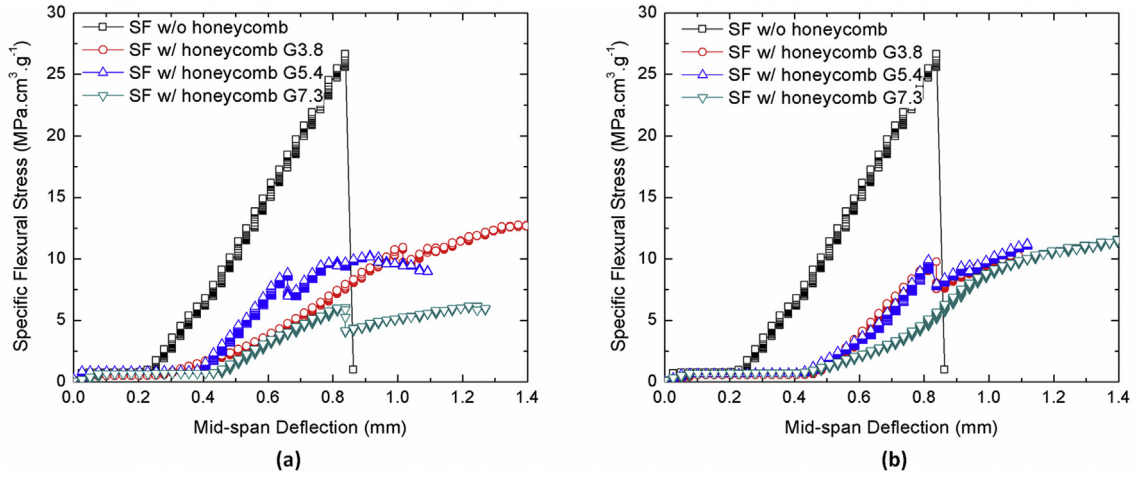

Fig. 13. Specific flexural strength of syntactic foam composites under in-plane 3-point bending (a) and out-of-plane 3-point bending (b).

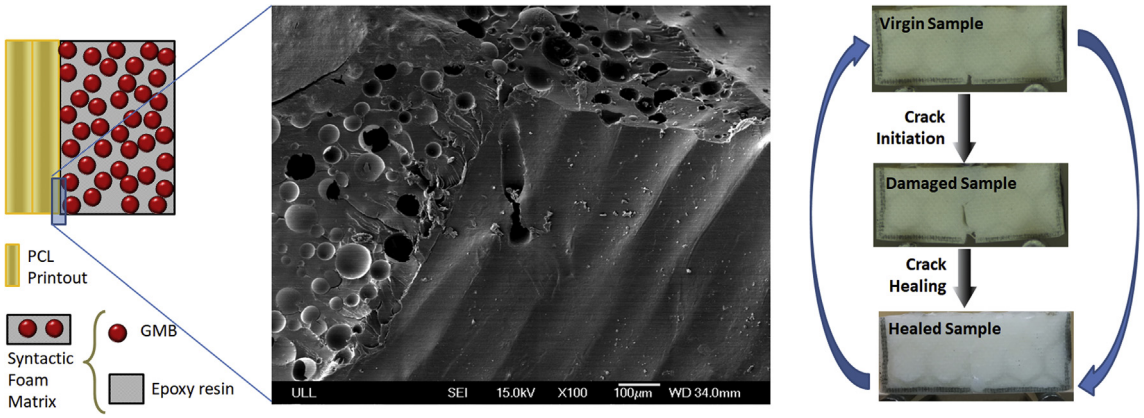

Fig. 14. Interface between PCL printout and syntactic foam matrix and the crack close-then-heal performance.

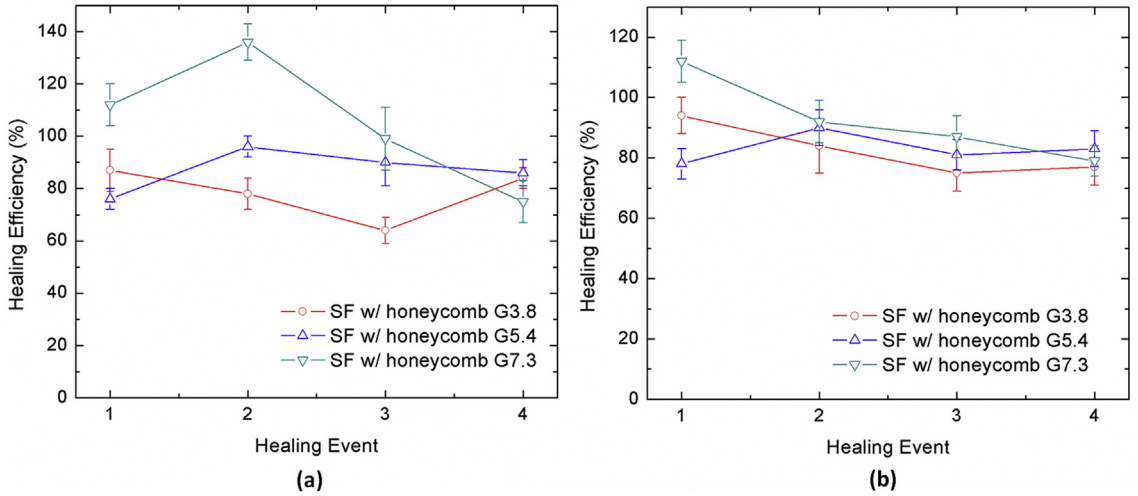

Fig. 15. Crack healing efficiency and repeatability of syntactic foam composites: (a) healing after in-plane bending damage; (b) healing after out-of-plane bending damage.

4. Conclusion

In this study, a novel grid skeleton (i.e., the 3D printed PCL honeycomb structure) was embedded in a syntactic foam matrix to enable the composites to own crack closing and healing capabilities. The volume fraction of GMB was constant, but the reinforced 3D printed honeycomb cell sizes were varied with a ratio from 3.8, to 5.4 and 7.3, which lead to different physical and mechanical properties such as the density and compressive strength. The interfaces between the syntactic foam matrix and PCL skeleton was investigated through FTIR analysis. It showed that the interaction between those phases were completely physical. Three-point bending tests were conducted to initiate structural level cracks, in order to examine the crack self-healing capability. Under free constraint condition, the 3D printed PCL honeycomb

reinforced syntactic foam exhibited promising crack healing performance with healing efficiencies above 80%. The reinforcement of 3D printed healing-agent based honeycomb structure provides a promising strategy for solving the structural property-healing efficiency trade-off problems. The future study on improving overall structural property and healing efficiency will be focused on the interface property between the 3D printout and matrix materials.

Acknowledgements

This work is financially supported by the College of Engineering at the University of Louisiana at Lafayette through the new faculty startup fund (No. 210125). The authors gratefully acknowledge Dr. David Hui (Department of Mechanical Engineering, University of New Orleans) for providing insightful comments and constructive suggestions during the revision of this manuscript.

Appendix A. Supplementary data

Supplementary data related to this article can be found at http://dx.doi.org/10.1016/j.compositesb.2018.06.005.

References

[1] Vance AP, Parks RM. Foam plastics in aircraft. J Cell Plast 1966;2:345–7.
[2] Hobaica EC, Cook SD. The characteristics of syntactic foams used for buoyance. J Cell Plast 1968;4:143–8.
[3] Anderson TF, Walters HA, Glesner CW. Castable, sprayable, low density foams and composites for furniture, marble, marine. J Cell Plast 1970;6:171–8.
[4] Manakari V, Parande G, Gupta N. Effects of hollow fly-ash particles on the properties of magnesium matrix syntactic foams: a review. Mater Perform Charact 2016;5:116–31.
[5] Gupta N, Woldesenbet E, Mensah P. Compression properties of syntactic foams: effect of cenosphere radius ratio and specimen aspect ratio. Composites Part A 2004;35:103–11.
[6] Vishwakarma A, Mondal DP, Birla S, Das S, Prasanth N. Effect of cenosphere size on the dry sliding wear behavior LM13-cenosphere syntactic foam. Tribol Int 2017;110:8–22.
[7] Wouterson EM, Boey FYC, Hu X, Wong SC. Specific properties and fracture toughness of syntactic foam: effect of foam microstructures. Compos Sci Technol 2005;65:1840–50.
[8] Li P, Petrinic N, Siviour CR, Froud R, Reed JM. Strain rate dependent compressive properties of glass microballoon epoxy syntactic foam. Mater Sci Eng, A 2009;515:19–25.
[9] Gupta N, Ye R, Porfiri M. Comparison of tensile and compressive characteristics of vinyl ester/glass microballoon syntactic foams. Composites Part B 2010;41:236–45.
[10] Zhang L, Ma J. Effect of coupling agent on mechanical properties of hollow carbon microsphere/phynolic resin syntactic foam. Compos Sci Technol 2010;70:1265–71.
[11] Hu G, Yu D. Tensile, thermal and dynamic mechanical properties of hollow polymer particle-filled epoxy syntactic foam. Mater Sci Eng, A 2011;528:5177–83.
[12] Wu X, Dong L, Zhang F, Zhou Y, Wang L, Wang D, Yin Y. Preparation and characterization of three phase epoxy syntactic foam filled with carbon fiber reinforced hollow epoxy macrospheres and hollow glass microspheres. Polym Compos 2016;37:497–502.
[13] Riessen AV. Thermo-mechanical and microstructural characterisation of sodium-poly (sialate-siloxo)(Na-PSS) geopolymers. J Mater Sci 2007;42:3117–23.
[14] Liu MYJ, Alengaram UJ, Jumaat MZ, Mo KZ. Evaluation of thermal conductivity, mechanical and transport properties of lightweight aggregate foamed geopolymer concrete. Energy Build 2014;72:238–45.
[15] Jiang B, Peng B, Zhu A, Zhang C, Li Y. Eco-friendly synthesis of graphene nanoplatelets via a carbonation route and its reinforcement for polytetrafluoroethylene composites. J Mater Sci 2018;53:626–36.
[16] Swetha C, Kumar R. Quasi-static uni-axial compression behavior of hollow glass microspheres/epoxy based syntactic foams. Mater Des 2011;32:4152–63.
[17] Huang R, Li P. Elastic behavior and failure mechanism in epoxy syntactic foams: the effect of glass microballoon volume fractions. Composites Part B 2015;78:401–8.
[18] Yu Q, Zhao Y, Dong A, Li Y. Mechanical properties of EPS filled syntactic foams prepared by VARTM. Composites Part B 2018;136:126–34.
[19] Zhang P, Li G. Advances in healing-on-demand polymers and polymer composites. Prog Polym Sci 2016;57:32–63.
[20] Bekas DG, Tsirka K, Baltzis D, Paipetis AS. Self-healing materials: a review of advances in materials, evaluation, characterization and monitoring techniques. Composites Part B 2016;87:92–119.
[21] Tavangarian F, Hui D, Li G. Crack-healing in ceramics. Composites Part B 2018;144:56–87.
[22] Lee J, Bhattacharyya D, Zhang MQ, Yuan YC. Mechanical properties of a self-healing fibre reinforced epoxy composites. Composites Part B 2015;78:515–9.
[23] Li G, John M. A self-healing smart syntactic foam under multiple impacts. Compos Sci Technol 2008;68:3337–43.
[24] Li G, Uppu N. Shape memory polymer based self-healing syntactic foam: 3-D confined thermomechanical characterization. Compos Sci Technol 2010;70:1419–27.
[25] Li G, Nettles D. Thermomechanical characterization of a shape memory polymer based self-repairing syntactic foam. Polymer 2010;51:755–62.
[26] Champagne J, Pang SS, Li G. Effect of confinement level and local heating on healing efficiency of self-healing particulate composites. Composites Part B 2016;97:344–52.
[27] Zhang P, Ogunmekan B, Ibekwe S, Jerro D, Pang SS, Li G. Healing of shape memory polyurethane fiber reinforced syntactic foam subjected to tensile stress. J Intell Mater Syst Struct 2016;27:1792–801.
[28] John M, Li G. Self-healing of sandwich structures with a grid stiffened shape memory polymer syntactic foam core. Smart Mater Struct 2010;19:075013.
[29] Olsson R. Mass criterion for wave controlled impact response of composite plates. Composites Part A 2000;31:879–87.
[30] Li G, Muthyala VD. Impact characterization of sandwich structures with an integrated orthogrid stiffened syntactic foam core. Compos Sci Technol 2008;68:2078–84.
[31] Zhang P, Li G. Healing-on-demand composites based on polymer artificial muscle. Polymer 2015;64:29–38.
[32] Zhang P, Ayaugbokor U, Ibekwe S, Jerro D, Pang SS, Mensah P, Li G. Healing of polymeric artificial muscle reinforced ionomer composite by resistive heating. J Appl Polym Sci 2016. http://dx.doi.org/10.1002/app.43660.
[33] Zhang P, Li G. Fishing line artificial muscle reinforced composite for impact mitigation and on-demand damage healing. J Compos Mater 2016. http://dx.doi.org/10.1177/0021998316636454.
[34] Wei H, Yao Y, Liu Y, Leng J. A dual-functional polymeric system combining shape memory with self-healing properties. Composites Part B 2015;83:7–13.
[35] Luo X, Mather PT. Shape memory assisted self-healing coating. ACS Macro Lett 2013;2:152–6.
[36] Wang X, Jiang M, Zhou Z, Gou J, Hui D. 3D printing of polymer matrix composites: a review and prospective. Composites Part B 2017;110:442–58.
[37] Zhang P, Arceneaux DJ, Khattab A. Mechanical properties of 3D printed polycaprolactone honeycomb structure. J Appl Polym Sci 2017. http://dx.doi.org/10.1002/app.46018.
[38] Mawhinney DB, Glass JA, Yates JT. FTIR study of the oxidation of porous silicon. J Phys Chem B 1997;101:1202–6.
[39] Yu J, Wu P. Crystallization process of poly(ε-caprolactone)-poly(ethylene oxide)-poly(ε-caprolactone) investigated by infrared and two-dimensional infrared correlation spectroscopy. Polymer 2007;48:3477–85.
[40] Zain NM, Ahmed SH, Ali ES, Zubir SA, Ahad NA. Characteristics of hydrolysis resistant polycaprolactone/palm kernel oil based polyol. Adv Mater Res 2012;576:334–7.
[41] Colloca M, Nikhil Gupta, Porfiri M. Tensile properties of carbon nanofiber reinforced multiscale syntactic foams. Composites Part B 2013;44:584–91.
[42] Li G, Zhang P. A self-healing particulate composite reinforced with short strain-hardened shape-memory polyurethane fibers. Polymer 2013;54:5075–86.
[43] Dyskin AV, Estrin Y, Kanel-Belov AJ, Pasternak E. A new principle in design of composite materials: reinforcement by interlocked elements. Compos Sci Technol 2003;63:483–91.
[44] Zhang J, Ashby MF. The out-of-plane properties of honeycombs. Int J Mech Sci 1992;34:475–89.
[45] Gibson LJ, Ashby MF. Cellular solids: structure and properties. Oxford: Pergamon Press; 1988.